THE JOURNAL OF PHYSICAL CHEMISTRY A

pubs.acs.org/JPCA Article

# Electron Scattering Cross Sections for Anthracene and Pyrene

Suvam Singh,* Dhanoj Gupta, Bobby Antony, Maria Tudorovskaya, and Jonathan Tennyson

Cite This: J. Phys. Chem. A 2020, 124, 7088−7100 Read Online

ACCESS | Metrics & More | Article Recommendations

**ABSTRACT:** UK molecular R-matrix calculations have been carried out for electron scattering from anthracene and pyrene. These molecules belong to the family of polycyclic hydrocarbons (PAHs) and are found in a nebula known as the Red Rectangle. Static exchange (SE), static exchange plus polarization (SEP), and close coupling (CC) approximations are used for scattering calculations. Different elastic and inelastic cross sections are computed in the present work in the energy range of 0.1−15 eV. Dissociative electron attachment cross sections are also calculated for both the molecules. Various shape, Feshbach/core-excited, and mixed resonances are detected for these molecules below 10 eV. All of the resonances detected in the present study are in agreement with the existing experimental and theoretical results. Due to the complexity of the present targets, electron collision cross sections are essentially unknown and hence most of the results are presented for the first time.

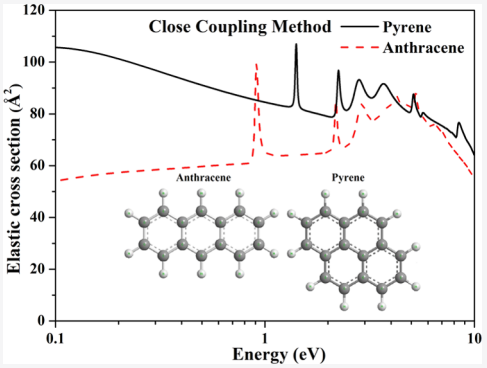


## INTRODUCTION

Electron scattering study of cyclic compounds is a trending topic,[1−6] among which polycyclic aromatic hydrocarbons (PAHs) form an interesting set of targets to analyze electron scattering processes. The emissions of infrared light from PAHs are shreds of evidence, which indicate that these molecules are present in large quantities in deep space. The carbon and hydrogen atoms are believed to get captured in the stellar wind, which is then blown out to form the nebula. These gases cool down to form bigger and bigger molecules as in PAHs. Anthracene and pyrene have been recently detected in a nebula called the Red Rectangle,[7] which is about a thousand light years from the Earth, suggesting that this mechanism actually operates. Anthracene is also found in a thick cloud toward the star Cernis 52 in Perseus, approximately 700 light years away from the Sun.[8] PAHs have long been suggested as the source of the ubiquitous diffuse interstellar bands (DIBs),[9] and the extensive distribution of PAHs in space means that it is quite likely that they might have played a role in the formation of many organic molecules present during the evolution of the solar system. Organic molecules like anthracene and pyrene are prebiotic, and when these organic molecules combine with ammonia and water in presence of ultraviolet radiation, they tend to produce amino acids and other essential compounds that are considered important for the development of life.[10] Hence, it has been suggested that the presence of these organic molecules on the early Earth may have helped in the origin of life. The oxidized forms of anthracene are biochemically very active and common in living systems. On the other hand, pyrene is the smallest hydrocarbon that exhibits a 5−7 member ring defect, which is found to have a significant effect on the formation of large aromatic molecules in the interstellar medium (ISM), especially in the carbon-rich asymptotic giant branch stars.[11] PAHs are formed by various combinations of benzenoid rings containing $sp^2$-hybridized C atoms that have hydrogen atoms at the periphery of the molecule where the carbon bonds get terminated. The remaining delocalized electrons together form $\pi$-bonds over the C atoms.[12] These $\pi$-bonds make the PAHs less vulnerable to disruption by ultraviolet rays, which offers them the essential stability to survive in high radiation environments in which they are likely to be found.[13] However, small PAHs like anthracene and pyrene are produced from disruption of larger PAH complexes in the harsh interstellar environment. Continuous destruction of PAHs is considered to be one of the important processes in the evolution of the interstellar medium, which involves the understanding of galaxy formation.[14]

The allotropes of carbon are responsible for the heating of interstellar gases because they are one of the main suppliers of free electrons in the interstellar clouds.[13] Hence, the study of electron collisions from the PAH molecules proves to be important in many astrophysical environments. Interstellar ruminants and various ISM shocks produce energetic electrons having energy from a few electron volts to several hundreds of giga-electron volts.[12] These energetic electrons form an

Received: June 19, 2020
Revised: August 7, 2020
Published: August 10, 2020







https://dx.doi.org/10.1021/acs.jpca.0c05589
J. Phys. Chem. A 2020, 124, 7088−7100

important constituent of cosmic rays and thus of the interstellar medium. However, the detection of these low-energy spectra is not viable even with far-ranging spacecraft due to the fact that most of them are slowed down by solar winds. As the energy of these energetic electrons increases, their intensity falls off rather sharply. Thus, the study of the low-energy spectrum of energetic electrons is important. Such a study could reveal the interaction mechanism of the energetic electrons with the interstellar components (here PAH molecules), which offer important inputs to various astrophysical models.

In the present work, R-matrix calculations[4,15,16] for electron scattering from two PAHs—anthracene and pyrene—are undertaken. The aforementioned reasons and applications form the main motivation to carry out the present work. The calculation of such big molecules is quite intricate using the *ab initio* R-matrix method. However, due to the symmetrical nature of these molecules, we could perform many calculations with various target models to get an idea about the convergence of the results. Finally, all of the results are presented for the best target model. Electron scattering total elastic cross sections ($Q_{el}$) along with the cross sections of its symmetry components are presented in this article. In addition to that, electron excitation cross sections ($Q_{exc}$) for various excited states are also calculated. Moreover, a comparative study is also done between various cross sections of the two molecules, which include the calculation of dissociative electron attachment (DEA) cross sections. Anthracene and pyrene are solids at room temperature, which is why experiments are very difficult to perform. This could well be the reason for the lone experimental results available, which are due to Burrow et al.[17] They provided the resonance positions for electron scattering from anthracene. Hence, the present study is an important step toward an understanding of various mechanisms of electron scattering from these molecules. According to our knowledge, Sanz et al.[18,19] is the only group who have performed calculations on electron scattering from anthracene. In one of their articles,[18] they have presented a complete set of integral cross sections from 0.00001 to 10 000 eV, while in their other article[19] they have studied various resonant states for anthracene. They have used e-POLYSCAT and IAM-SCAR (independent atom model-screening-corrected additivity rule) methods for their calculations. We compare our results with those of Sanz et al.[18,19] and find modest agreement in most of the cases. However, we have not found any electron scattering study related to pyrene; hence, this article reports data on this for the first time. In the present work, we employ static exchange (SE), static exchange plus polarization (SEP), and close coupling (CC) approximations for the scattering calculations. The respective results are also compared with each other.

The Theory section gives a gist of the theoretical methods applied along with the target model used to carry out the present work. The results are discussed in the Results and Discussion section, and then, the conclusions are drawn in the Conclusions section.

## THEORY

The UK molecular R-matrix method[4,15,16] driven by the Quantemol-N package[20] is employed in the present calculations. The review article by Tennyson[16] provides a thorough explanation of the UK molecular R-matrix codes employed. This section gives a brief description of the theory along with the detailed target models used in this work.

All calculations presented here are executed under the fixed-nuclei (FN) approximation, where nuclear motion is not taken into consideration. The electron−molecule interaction space is divided into two regions: an inner region and an outer region, which are separated by a sphere of radius '$r$' taken from the center of mass of the molecule. To guarantee a good calculation, we need to make sure that all of the charge densities of the target molecule are contained within this R-matrix sphere as well as they should also be large enough to include all of the orbitals used to build the $L^2$ functions. In the present calculations, the R-matrix radius of $13a_0$ is taken for both anthracene and pyrene, while the outer region was propagated up to $100a_0$. The inner region includes exchange and polarization correlation effects, whereas the outer region neglects these interactions and considers the long-range multipolar potential of the target−electron system. The wavefunction of the target−electron system in the inner region is represented by the CC expansion, which is given as the linear combination of two terms

$$\psi_k^{N+1} = A \sum_{ij} \Phi_i(x_N;\ \hat{r}_{N+1};\ \sigma_{N+1}) \frac{u_{ij}(r_{N+1})}{r_{N+1}} a_{ijk} + \sum_i \chi_i(x_{N+1}) b_{ik} \quad (1)$$

Here, $A$ stands for the antisymmetrization operator and $\Phi_i$ gives electronic wavefunction of the $i$th state of the $N$-electron system. $x_N$ and $x_{N+1}$ denote the space and spin coordinates of the $N$ and $N + 1$ electron systems and $\hat{r}_{N+1}$ and $r_{N+1}$ are the angular and radial coordinates, respectively, of the $(N + 1)$th electron. $\sigma_{N+1}$ gives the spin of the scattering electron. $\frac{u_{ij}(r_{N+1})}{r_{N+1}}$ is a function that describes the wavefunction of the scattering electron. The $\chi_i$'s are short-range $L^2$-integrable functions where the scattering electron occupies a target orbital. These configurations are important for a number of reasons and, in particular, help to provide a good description of the short-range polarization in the SEP and CC models. $a_{ijk}$ and $b_{ik}$ are the coefficients derived by the condition that the wavefunction in eq 1 diagonalizes the nonrelativistic Hamiltonian of the $(N + 1)$-electron system.

In the outer region, the physics is much simpler compared to that in the inner region, and the interaction between the incident electron and the target is approximated by a single-center multipole potential expansion. The energy-independent inner region wavefunctions $\psi_k^{N+1}$ are used for the construction of the R-matrix at the boundary between the two regions. This R-matrix is propagated to the asymptotic region to evaluate the K-matrix by matching asymptotic solutions of Gailitis expansion.[21] From K-matrices, one can obtain T-matrices, which are further used to determine scattering cross sections and extract positions and widths of resonances if any. The module RESON[22] is used to detect resonances, which it fits to a Breit−Wigner profile. The POLYDCS code of Sanna and Gianturco[23] is employed for the calculation of differential cross sections, and the binary encounter Bethe (BEB) model[24] is utilized for the computation of ionization cross sections. The complete molecular orbitals are constructed with the help of Gaussian-type orbitals, while the continuum orbitals are used from the work of Faure et al.[25] that includes partial waves up to


https://dx.doi.org/10.1021/acs.jpca.0c05589
J. Phys. Chem. A 2020, 124, 7088−7100

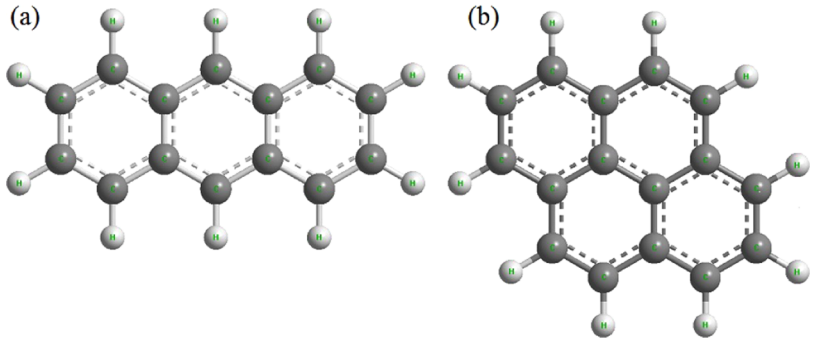


**Figure 1.** Structures of (a) anthracene and (b) pyrene.

$g$ waves ($l$ = 4), which is sufficient for molecules having no permanent dipole moment.

The type of scattering model depends on the choice of target electronic states and $L^2$ functions included in eq 1. In this work, SE, SEP, and CC models are used for scattering calculations. In the SE model, the target wavefunction is frozen in its Hartree−Fock (HF) ground state and is not allowed to be polarized by the incident electron. This method is used to calculate only elastic scattering cross sections. Moreover, this method is well suited for detecting shape resonances, where the scattering electron is temporarily trapped behind a potential barrier created by the molecule. The SE approximation cannot detect Feshbach/core-excited or mixed resonances, which involve excitation of bound electrons. The SEP approximation builds on the SE model by accounting for polarization effects by including $L^2$ configurations involving single excitations from the HF target wavefunction. The SEP model is found to be particularly good at describing shape resonances; this method can also describe core-excited resonances such as Feshbach resonances, which are associated with single excitations of the target molecule but are prone to also give false (pseudo) resonances at collision energies above the first electronic excitation threshold. Modeling resonances (particularly shape ones) at SE and SEP levels in R-matrix calculations are strongly dependent on the virtual orbitals used to construct the $L^2$ configurations.[26] The CC approximation is a sophisticated approximation, where many electronically excited states of the target are included in the expansion of eq 1. The inclusion of more excited states allows for both polarization effects and the loss of flux into an electronically excited state; this makes these calculations accurate at higher energies. CC calculations identify both the shape and Feshbach/core-excited resonances fairly well along with the calculation of excitation cross sections. The following subsection describes the target model used in the present calculations.

**Target Models for Anthracene ($C_{14}H_{10}$) and Pyrene ($C_{16}H_{10}$).** Figure 1(a) and 1(b) shows the structures of anthracene and pyrene, respectively. Anthracene is formed by three linearly condensed rings that consist of three fused benzene rings, whereas pyrene is an aromatic hydrocarbon consisting of four fused benzene rings, both belonging to the $D_{2h}$ point group symmetry. There are 94 and 106 electrons in anthracene and pyrene, respectively, and the neutral state was taken for their respective calculations. The Cartesian coordinates of both the molecules are taken from CCCBDB (Computational Chemistry Comparison and Benchmark DataBase)[27] optimized at the configuration interaction singles and doubles (CISD) level of approximation using the cc-pVDZ basis set. We have performed the Hartree−Fock (HF) and complete active space-configuration space (CAS-CI) calculations using the cc-pVDZ basis set for both the molecules. The target properties calculated from these approximations are given in Table 1. The HF approximation does not model the excited states well, whereas the CAS-CI model treats the excited states and hence the absolute value of the ground state energy is lower in the case of the CAS-CI model. The HF electronic ground state configuration of anthracene in its equilibrium geometry is given as $1b_{1u}^2$, $1b_{3g}^2$, $1a_g^2$, $1b_{2u}^2$, $2a_g^2$, $2b_{2u}^2$, $2b_{1u}^2$, $2b_{3g}^2$, $3b_{2u}^2$, $3a_g^2$, $3b_{3g}^2$, $3b_{1u}^2$, $4a_g^2$, $4b_{1u}^2$, $5a_g^2$, $4b_{2u}^2$, $6a_g^2$, $5b_{1u}^2$, $4b_{3g}^2$, $5b_{2u}^2$, $6b_{1u}^2$, $7a_g^2$, $5b_{3g}^2$, $6b_{2u}^2$, $8a_g^2$, $7b_{1u}^2$, $7b_{2u}^2$, $9a_g^2$, $6b_{3g}^2$, $10a_g^2$, $8b_{1u}^2$, $8b_{2u}^2$, $7b_{3g}^2$, $9b_{1u}^2$, $1b_{3u}^2$, $9b_{2u}^2$, $10b_{1u}^2$, $11a_g^2$, $1b_{1g}^2$, $8b_{3g}^2$, $12a_g^2$, $10b_{2u}^2$, $2b_{3u}^2$, $1b_{2g}^2$, $1a_u^2$, $2b_{1g}^2$, $2b_{2g}^2$, while that of pyrene is $1a_g^2$, $1b_{1u}^2$, $1b_{3g}^2$, $1b_{2u}^2$, $2a_g^2$, $2b_{1u}^2$, $2b_{2u}^2$, $3a_g^2$, $2b_{3g}^2$, $3b_{1u}^2$, $4a_g^2$, $4b_{1u}^2$, $3b_{2u}^2$, $3b_{3g}^2$, $5a_g^2$, $5b_{1u}^2$, $6a_g^2$, $6b_{1u}^2$, $4b_{2u}^2$, $7a_g^2$, $4b_{3g}^2$, $8a_g^2$, $7b_{1u}^2$, $5b_{2u}^2$, $9a_g^2$, $5b_{3g}^2$, $8b_{1u}^2$, $6b_{2u}^2$, $9b_{1u}^2$, $10a_g^2$, $6b_{3g}^2$, $7b_{2u}^2$, $11a_g^2$, $10b_{1u}^2$, $12a_g^2$, $7b_{3g}^2$, $8b_{2u}^2$, $13a_g^2$, $11b_{1u}^2$, $9b_{2u}^2$, $1b_{3u}^2$, $8b_{3g}^2$, $12b_{1u}^2$, $10b_{2u}^2$, $1b_{2g}^2$, $14a_g^2$, $1b_{1g}^2$, $9b_{3g}^2$, $2b_{3u}^2$, $1a_u^2$, $3b_{3u}^2$, $2b_{2g}^2$, $2b_{1g}^2$. In the case of anthracene, out of 94 electrons of the target, 86 electrons were kept frozen in $1a_g$, $2a_g$, $3a_g$, $4a_g$, $5a_g$, $6a_g$, $7a_g$, $8a_g$, $9a_g$, $10a_g$, $11a_g$, $12a_g$, $1b_{3u}$, $2b_{3u}$, $1b_{2u}$, $2b_{2u}$, $3b_{2u}$, $4b_{2u}$, $5b_{2u}$, $6b_{2u}$, $7b_{2u}$, $8b_{2u}$, $9b_{2u}$, $10b_{2u}$, $1b_{1g}$, $1b_{1u}$, $2b_{1u}$, $3b_{1u}$, $4b_{1u}$, $5b_{1u}$, $6b_{1u}$, $7b_{1u}$, $8b_{1u}$, $9b_{1u}$, $10b_{1u}$, $1b_{3g}$, $2b_{3g}$, $3b_{3g}$, $4b_{3g}$, $5b_{3g}$, $6b_{3g}$, $7b_{3g}$, and $8b_{3g}$ and the remaining 8 electrons were kept in active space in $13a_g$, $3b_{3u}$, $4b_{3u}$, $11b_{2u}$, $2b_{1g}$, $3b_{1g}$, $1b_{2g}$, $2b_{2g}$, $1a_u$, and $2a_u$ orbitals. For pyrene, out of 106 electrons of the target, 98 electrons were kept frozen in $1a_g$, $2a_g$, $3a_g$, $4a_g$, $5a_g$, $6a_g$, $7a_g$, $8a_g$, $9a_g$, $10a_g$, $11a_g$, $12a_g$, $13a_g$, $14a_g$, $1b_{3u}$, $2b_{3u}$, $1b_{2u}$, $2b_{2u}$, $3b_{2u}$, $4b_{2u}$, $5b_{2u}$, $6b_{2u}$, $7b_{2u}$, $8b_{2u}$, $9b_{2u}$, $10b_{2u}$, $1b_{1g}$, $1b_{1u}$, $2b_{1u}$, $3b_{1u}$, $4b_{1u}$, $5b_{1u}$, $6b_{1u}$, $7b_{1u}$, $8b_{1u}$, $9b_{1u}$, $10b_{1u}$, $11b_{1u}$, $12b_{1u}$, $1b_{2g}$, $1b_{3g}$, $2b_{3g}$, $3b_{3g}$, $4b_{3g}$, $5b_{3g}$, $6b_{3g}$, $7b_{3g}$, $8b_{3g}$, and $9b_{3g}$ and the remaining 8 electrons were kept in active space in $15a_g$, $3b_{3u}$, $4b_{3u}$, $2b_{1g}$, $3b_{1g}$, $13b_{1u}$, $2b_{2g}$, $3b_{2g}$, $1a_u$, and $2a_u$ orbitals. The first 20 target excited states for anthracene and pyrene are presented in Table 2. The scattering calculations were performed using the SE, SEP, and CC

**Table 1. Target Properties for Anthracene and Pyrene Obtained Using the CC Approximation with the cc-pVDZ Basis Set**

| target | method | ground state energy (Hartree) | ionization energy (eV) | rotational constant ($cm^{-1}$) |
|---|---|---|---|---|
| anthracene | HF | −534.741 | 7.32 | 0.073 |
| | CAS-CI | −534.794 | | |
| pyrene | HF | −611.812 | 7.14 | 0.034 |
| | CAS-CI | −611.858 | | |


https://dx.doi.org/10.1021/acs.jpca.0c05589
J. Phys. Chem. A 2020, 124, 7088−7100

**Table 2. Vertical Excitation Energies (in eV) for Anthracene and Pyrene Obtained Using the CAS-CI Model with the cc-pVDZ Basis Set for the 20 Low-Lying Excited States**

| anthracene | | | | pyrene | | | |
|---|---|---|---|---|---|---|---|
| state | energy | state | energy | state | energy | state | energy |
| $^1A_g$ | 0 | $^3B_{3g}$ | 6.936 | $^1A_g$ | 0 | $^1A_g$ | 6.479 |
| $^3B_{1u}$ | 2.966 | $^1B_{3g}$ | 6.974 | $^3B_{1u}$ | 3.382 | $^1B_{3g}$ | 6.539 |
| $^3B_{3g}$ | 4.517 | $^1A_g$ | 6.998 | $^3B_{2u}$ | 4.928 | $^3B_{3g}$ | 6.544 |
| $^3B_{2u}$ | 5.077 | $^3A_g$ | 7.257 | $^3B_{2u}$ | 5.276 | $^3A_g$ | 6.604 |
| $^1B_{1u}$ | 5.099 | $^1B_{2u}$ | 7.466 | $^3B_{3g}$ | 5.278 | $^1B_{2u}$ | 6.753 |
| $^3B_{1u}$ | 5.322 | $^1B_{1u}$ | 7.632 | $^3A_g$ | 5.320 | $^3B_{1u}$ | 6.914 |
| $^3B_{2u}$ | 5.532 | $^3B_{1u}$ | 7.727 | $^1B_{2u}$ | 5.344 | $^3A_g$ | 7.020 |
| $^1B_{2u}$ | 5.649 | $^1A_g$ | 7.774 | $^1B_{1u}$ | 5.415 | $^3B_{3g}$ | 7.072 |
| $^3B_{1u}$ | 6.220 | $^3A_g$ | 7.812 | $^3B_{1u}$ | 5.545 | $^1A_g$ | 7.311 |
| $^1B_{3g}$ | 6.715 | $^3B_{2u}$ | 7.877 | $^1B_{3g}$ | 6.133 | $^3A_g$ | 7.442 |

approximations for both the molecules. In the present endeavor, various tests were performed to check the convergence of the calculations. The convergence test was performed for anthracene, where we have used various target models by varying the R-matrix radius, changing the basis set, and also varying the number of target states in the CC approximation. We have shown the result of such study for the elastic cross section of anthracene in the Results and Discussion section. We finally chose the best target model with cc-pVDZ basis set with the R-matrix radius of $13a_0$ and 45 target state for all of the scattering cross section calculations. Since anthracene and pyrene belong to the same point group symmetry and have a similar structure, a similar model is used as for pyrene with the cc-pVDZ basis set with $13a_0$ radius and 48 target states. For both the molecules, the total number of configuration state functions (CSFs) generated for the ground state was 1860. A maximum of 185 and 173 scattering channels were used in the calculation for anthracene and pyrene, respectively.

## RESULTS AND DISCUSSION

Figure 2 shows the different tests to assess the convergence of the calculation. Various input parameters in the R-matrix calculation were varied to check their dependence on the scattering calculation. First, the R-matrix radius is optimized in Figure 2a. In this figure, the elastic cross section of anthracene is calculated by varying the R-matrix radius with the cc-pVDZ basis set and 45 target states. As evident from the figure, the cross sections are almost identical for the R-matrix radius of $a = 13a_0$ and $14a_0$. The result of using the $10a_0$ R-matrix radius is higher than all other results. Figure 2b shows the calculations for varying the basis sets with a fixed R-matrix radius of $13a_0$ and 45 target states. The cc-pVDZ basis calculation predicts the resonances at lower energies and with a lower magnitude of cross section than the DZP and 6-311G* basis sets. Similar behavior is seen in Figure 2c, where the cross sections seem to converge when larger number target excited states are used for the cc-pVDZ basis set with a radius of $13a_0$. From these three convergence tests, it is evident that our calculation shows convergence for the cc-pVDZ basis set at $13a_0$ R-matrix radius having 45 target excited states. Therefore, this model has been used to calculate all other cross sections for anthracene in the present study. A similar model is used for pyrene as well.

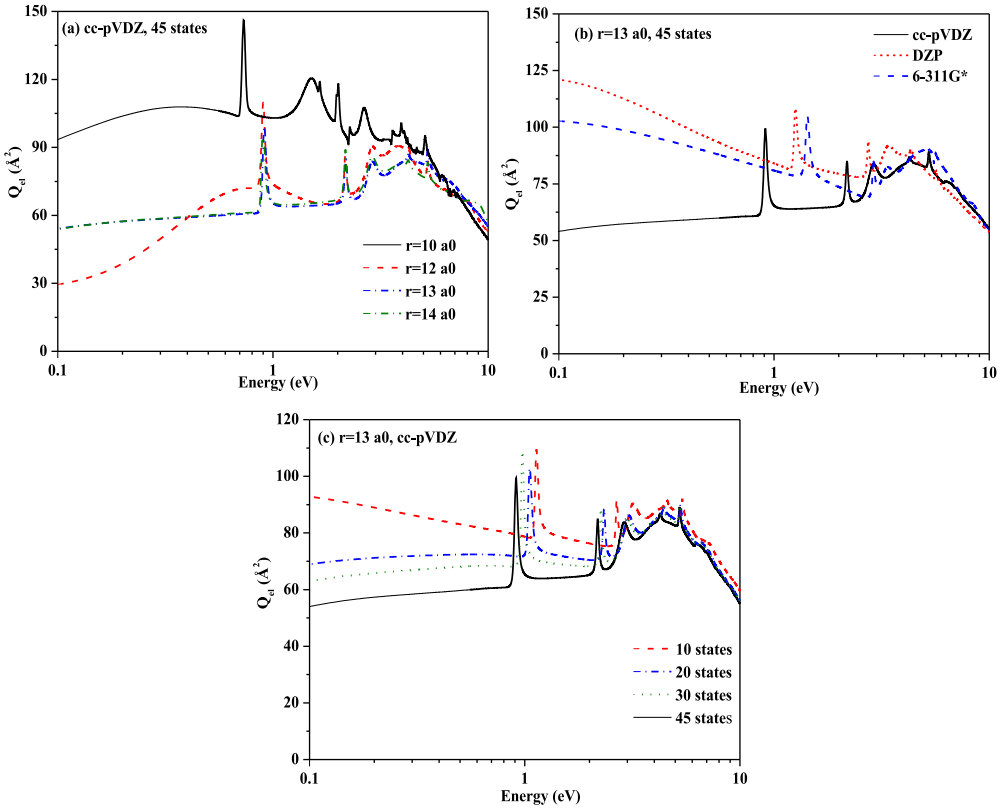


**Figure 2.** Elastic cross section for anthracene with (a) radius variation, (b) variation of basis sets, and (c) number of target excited states in a CC approximation.



https://dx.doi.org/10.1021/acs.jpca.0c05589
J. Phys. Chem. A 2020, 124, 7088−7100

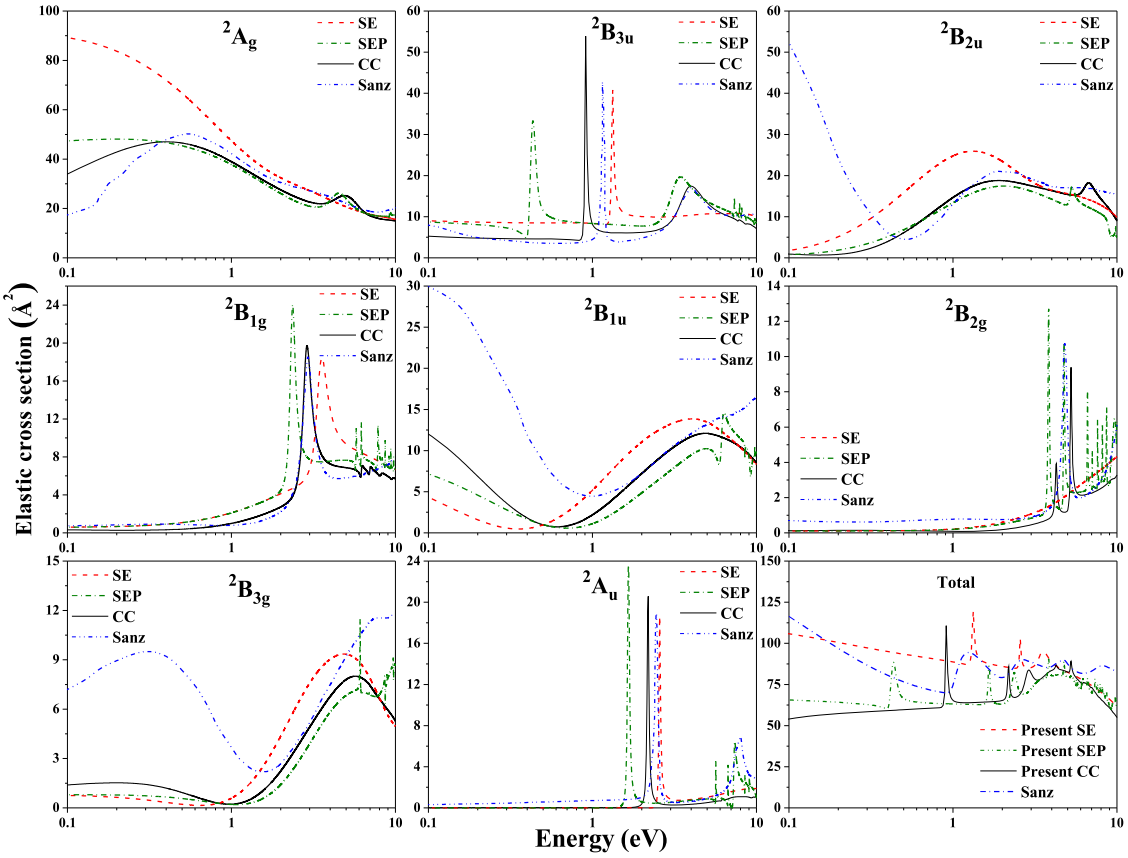


**Figure 3.** Symmetry components contributing to the elastic cross section for anthracene. The bottom right-hand panel shows the total elastic cross section. Dashed line, present SE approximation; dashed dot line, present SEP approximation; solid line, present CC approximation; dashed dot dot line, Sanz et al.[18]

**Table 3. Resonance Position and Width (in eV) for Anthracene at the SE, SEP, and CC Levels of Approximation in Comparison with the Data of Sanz et al.[19]**

| | present | | | | | | | | |
|---|---|---|---|---|---|---|---|---|---|
| | SE | | SEP | | CC | | Sanz et al[19] | | Burrow et al[17] |
| state | energy | width | energy | width | energy | width | energy | width | |
| $^2B_{3u}$ | 1.321 | 0.045 | 0.433 | 0.008 | 0.910 | 0.025 | 1.16 | 0.035 | 0.6 |
| $^2A_u$ | 2.566 | 0.064 | 1.657 | 0.045 | 2.180 | 0.062 | 2.46 | 0.098 | 1.5 |
| $^2B_{1g}$ | 3.462 | 0.649 | 2.343 | 0.208 | 2.847 | 0.402 | 2.91 | 0.51 | 1.67 |
| $^2B_{3u}$ | | | 3.151 | 1.199 | 3.662 | 1.607 | 3.76 | 1.974 | 1.8 |
| $^2B_{2g}$ | | | 3.828 | 0.0814 | 4.258 | 0.143 | 4.81 | 0.36 | 2.67 |
| $^2B_{2g}$ | | | 4.743 | 0.078 | 5.234 | 0.127 | | | |
| $^2B_{2u}$ | | | 5.251 | 0.382 | | | | | |
| $^2B_{1g}$ | | | 5.755 | 0.019 | 6.187 | 0.136 | | | |

Figure 3 presents the electron scattering $Q_{el}$ for anthracene due to all of the symmetry components as well as the total $Q_{el}$ along with the only comparison available from Sanz et al.[18] The R-matrix calculations are carried out using SE, SEP, and CC models. In the $Q_{el}$ calculated from the CC approximation, the first resonance is detected at 0.910 eV due to $^2B_{3u}$ symmetry. Further resonances are detected at positions 2.180, 2.847, 3.662, 4.258, 5.234 eV, and 6.187 due to symmetry states $^2A_u$, $^2B_{1g}$, $^2B_{3u}$, $^2B_{2g}$, $^2B_{2g}$, and $^2B_{1g}$, respectively. The details of the resonance position and width can be obtained from Table 3, where the present resonance data are compared with the recent theoretical data of Sanz et al.[19] and the experimental data of Burrow et al.[17] It is to be noted that the experimental resonance positions are compared according to the increase in the energies of their resonance position and not by symmetry as given by Sanz et al.[19] When compared with the theoretical data of Sanz et al.,[18] the maximum deviation in the position of the resonance is about ±0.55 eV (~13%), whereas the maximum deviation is around ±1.86 eV (~50%) when compared with the experimental data of Burrow et al.[17] Since the present calculations are based on the variational principle, the lower values of the energies compared to Sanz et al.[18] suggest that the present results may be better than those of Sanz et al.[18] In addition to that, they have also mentioned that in the low energies there is 10% uncertainty in their reported data. Burrow et al.[17] have also mentioned that the maximum uncertainty in their study is about 0.1 eV. The difference between the present resonance


https://dx.doi.org/10.1021/acs.jpca.0c05589
J. Phys. Chem. A 2020, 124, 7088−7100

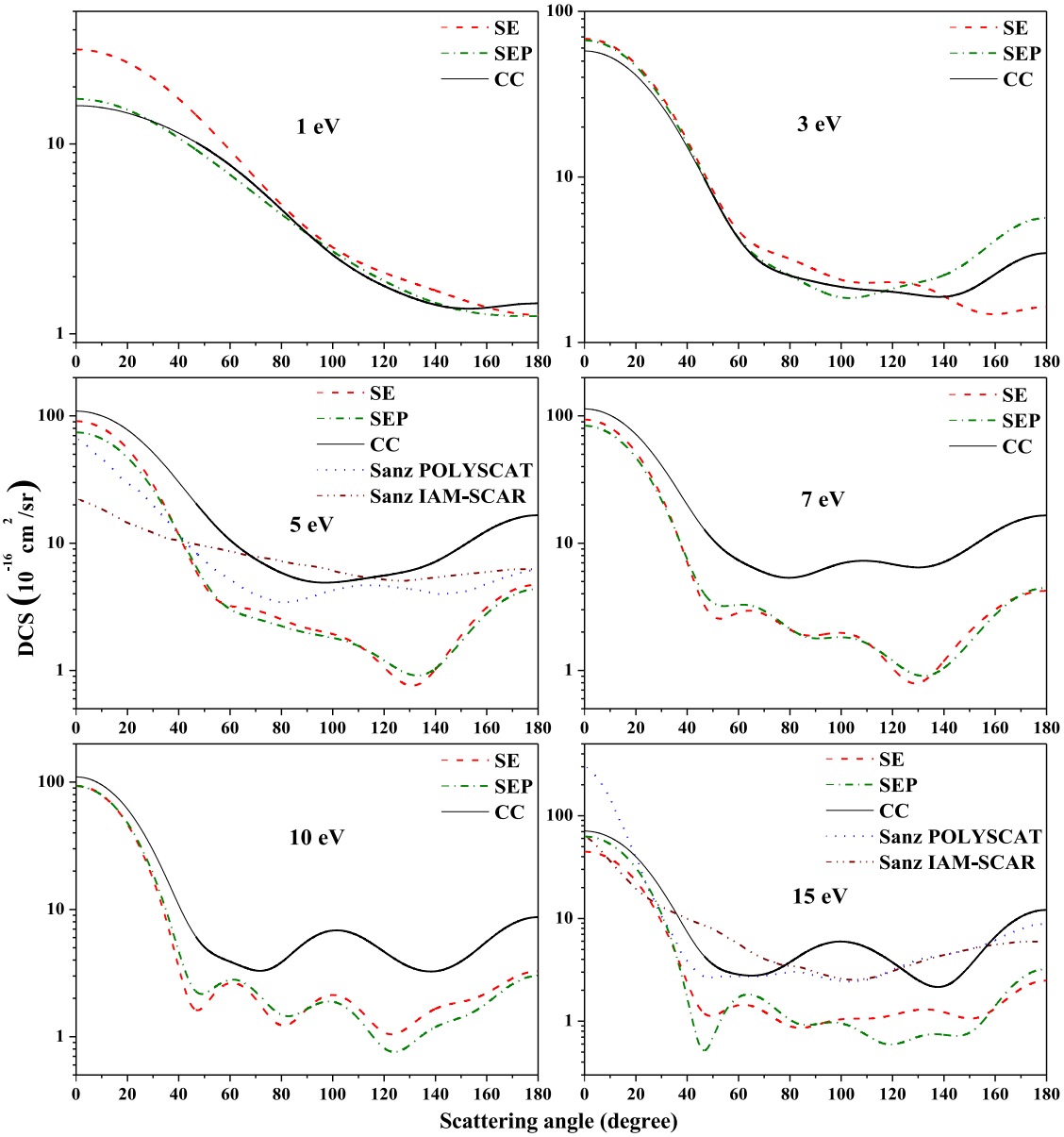


**Figure 4.** DCS for e-anthracene scattering for energies 1, 3, 5, 7, 10, and 15 eV. Dashed line, present SE approximation; dashed dot line, present SEP approximation; solid line, present CC approximation; dotted line, Sanz et al. POLYSCAT;[18] dashed dot dot line, Sanz et al. IAM-SCAR.[1818]

position and that of experimental data of Burrow et al.[17] may be due to two reasons; first, it may be that our results may not have fully converged and the other reason may be due to the effect of nuclear motion, which is not considered in the present calculations. Such nuclear motion allows for the relaxation of the molecule in the experiment.

Resonances detected in the present CC study due to different symmetries show good compliance with the resonances reported by Sanz et al.[19] Moreover, the detected resonances are at slightly lower energies compared to those by Sanz et al.[19] Furthermore, the present SEP approximation has detected all of the resonances at lower energies compared to CC and SE approximations. The resonances observed in the experiments of Burrow et al.[17] are in closer agreement with the SEP results than our CC and SE approximations and the results of Sanz et al.[19] This is likely due to the fact that the SEP approximation describes polarization effects better than the CC approximation and hence the resonance positions are lowered. All of the five resonances observed in the experiment of Burrow et al.[17] are also detected in the present study. The magnitude of the total elastic cross section in CC is lower than that in SE and SEP, which could be due to the loss of flux in various open channels that are available in various multistate calculations such as CC in the present case. Moreover, due to the inclusion of excited states, the CC calculation satisfactorily models the Feshbach and core-excited resonances, resulting in the observation of many such resonances near the threshold of the excited states. This is evident from the inelastic cross section of anthracene plotted in Figure 5, where many sharp peaks are seen in the excitation cross section for various excited states. The peaks are also visible in the elastic cross section of various symmetries plotted in Figure 3 in the CC model. The cross sections for all of the symmetries in the three SE, SEP, and CC models are plotted together along with the data of Sanz et al.[19] to get an idea about the position and width of the resonances and the magnitude of the cross section. As can be


https://dx.doi.org/10.1021/acs.jpca.0c05589
J. Phys. Chem. A 2020, 124, 7088−7100

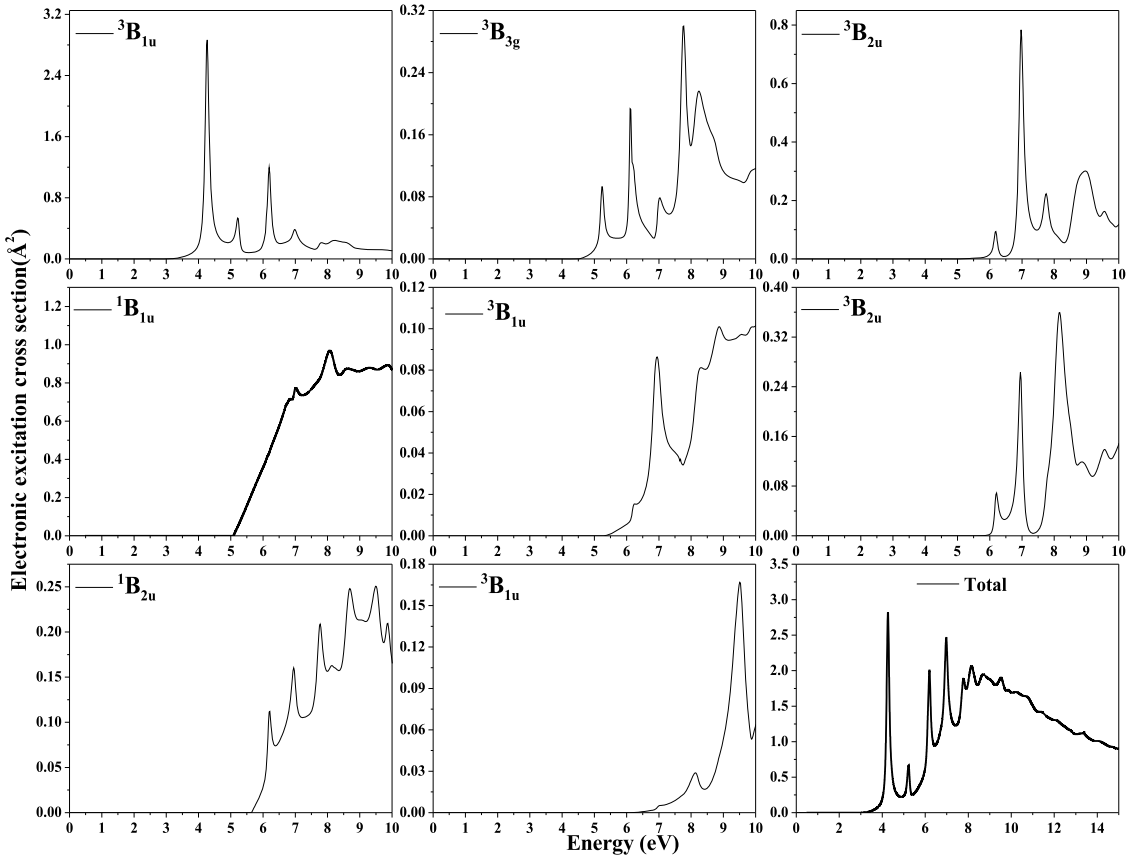


**Figure 5.** Electronic excitation cross section for anthracene for various low-lying excited states. The bottom right-hand panel shows the total electronic excitation cross section.

seen from the figure, the SEP model detects resonances at lower energies compared to all of the data. Three $\pi^*$ single-particle shape resonances are detected in the SE approximation in the present study due to $^2B_{3u}$, $^2A_u$, and $^2B_{1g}$ states. The SEP model has detected eight resonances in total in the present study below 6 eV. We believe that resonances appearing in the cross section above 6 eV may be pseudoresonances. The resonances detected in the SEP model are at 0.433, 1.657, 2.343, 3.151, 3.828, 4.743, 5.251, and 5.755 eV. The SEP calculation does not include the excited states of the target molecule, but in the $N + 1$ wavefunction, some of the configurations are required to describe excited states, which leads to the observation of some features that correspond to core-excited resonances.[28] Thus, in the SEP calculation, the lowest three resonances correspond to be of shape character. The resonances at higher energies are most likely to be core-excited shape resonances because in each case there are rather (very) broad resonances that are too broad to be straight Feshbach. The Feshbach/core-excited resonances are more elaborately and accurately described in the CC approximation, where the excited states are explicitly included in the calculation. In the CC approximation, we have detected seven resonances at 0.910, 2.180, 2.847, 3.662, 4.258, 5.234, and 6.187 eV, of which the first three are of shape character. The next two (according to energy) are too broad to be of Feshbach type, and hence, they are likely to be of core-excited shape resonance. The other two resonances may be of Feshbach/core-excited type; however, these resonances are not clearly identifiable. Owing to the complications of the present system, identifying the parent state of the Feshbach resonances is very unlikely to be straightforward. None of the resonances are sitting just below an excitation threshold (classic behavior for a Feshbach resonance and its parents) and it is likely that the resonances actually have multiple parents.[29] We are not able to clearly identify the type of resonances here, but the present results could be a useful guideline for future studies. Structures are also seen in the cross sections above 6 eV in the CC approximation, which are not detected as resonances. They are believed to be pseudoresonances that may have occurred due to the exclusion of a complete set of target states during the CC expansion of eq 1. Interestingly, a resonance is observed at 5.251 eV in the SEP curve for $^2B_{2u}$ symmetry, which is neither observed in SE nor in CC; hence, this resonance might be of mixed shape core-excited character. The $\pi^*$-type shape resonance suggests that the electron density is strongly localized on the carbon bonds associated with specified bonds, which result in a paucity of the electron density on the terminal hydrogen atoms. The lack of electron density on the H atom indicates that it may be a possible path of fragmentation that is often observed in aromatic systems. Now, if one H atom detaches from anthracene, the foliage of dehydrogenated anionic radical $C_{14}H_9^-$ of anthracene is left. Since all of the resonances detected below the first excitation threshold are $\pi^*$-type in nature, it is highly unlikely that these resonances will lead to ring-breaking fragmentations. On the other hand, since $\pi^*$-type resonances are somewhat weakly coupled to the nuclear motions of the neutral partner in polycondensed aromatic rings, there are possibilities that such types of resonances will produce diffuse energy rearrangements within the molecular model before getting autodetached. To


https://dx.doi.org/10.1021/acs.jpca.0c05589
J. Phys. Chem. A 2020, 124, 7088−7100

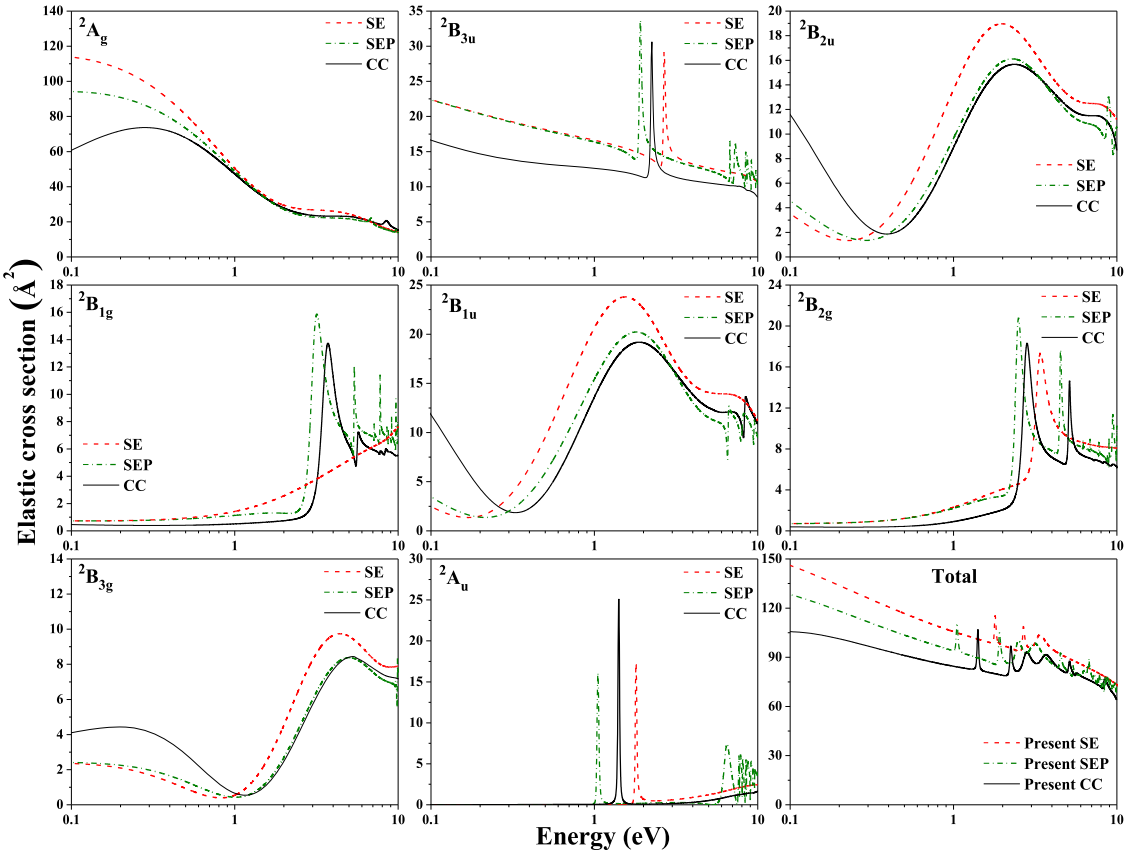


**Figure 6.** Symmetry components contributing to the elastic cross section for pyrene. The bottom right-hand panel shows the total elastic cross section. Dashed line, present SE approximation; dashed dot line, present SEP approximation; solid line, present CC approximation.

study these processes in some detail, a brief DEA investigation is made in the later part of this article.

DCSs for anthracene at incident electron energies of 1, 3, 5, 7, 10, and 15 eV are shown in Figure 4. Similar to previous cases, the calculations are performed using three different approximations of SE, SEP, and CC. The SE and SEP models predict comparable values in almost all of the cases. This could be due to the fact that SE and SEP models have the same number of channels included in the computation. The calculations based on the CC model give higher cross sections in a number of cases. This might be attributed to the nature of the potentials used here. The SE model only has static potential, whereas SEP and CC models also allows for polarization. In general, the static potential is repulsive, while the polarization potential is attractive so they partially cancel each other, which leads to smaller cross sections. However, this cancellation is less straightforward in multichannel problems and seems not to be occurring in the case of CC calculations. Hence, larger cross sections are observed for CC. The results obtained from these models are compared with the only available data of Sanz et al.[18] at 5 and 15 eV. At 5 eV, the present CC results show reasonable agreement with the e-POLYSCAT data of Sanz et al.[18] for all scattering angles. Such an agreement at the lower energies suggests similar modeling of polarization and electron correlation in both works. At 15 eV, our CC DCS also agrees well with the e-POLYSCAT data of Sanz et al.[18] However, in this energy range, many inelastic channels are open, leading to incorrect results by the use of K-matrices. This could be the main reason that heavy oscillations are observed at 10 and 15 eV. This is also one of the reasons for the difference between DCS calculated using the CC approximation compared to the SE and SEP approximations at higher energies. The oscillatory nature of the curve might also occur due to destructive interference among various partial wave amplitudes.

Figure 5 depicts the electron scattering $Q_{exc}$ for the first eight excited states for anthracene. The bottom right panel shows the total $Q_{exc}$. The threshold for the first vertical excitation is at 2.966 eV for the $^3B_{1u}$ scattering state. This state is also responsible for the highest contribution in the total $Q_{exc}$ with a maximum magnitude of 2.86 Å$^2$. The first 20 vertical excited states are provided in Table 2. A number of peaks are observed in the total $Q_{exc}$ plot; the first three peaks at 4.258, 5.216, and 6.190 eV can be associated with the resonances detected in our CC calculation. All of these resonances detected above the first excitation threshold are probably of Feshbach/core-excited nature, which is consistent with the same not appearing in the SE calculations. The peak at 4.258 eV has a major contribution from the $^3B_{1u}$ scattering state, whereas peaks at 5.216 and 6.184 eV have contributions from scattering states $^3B_{1u}$, $^3B_{3g}$ and $^3B_{1u}$, $^3B_{2u}$ respectively.

Figure 6 presents the elastic scattering cross sections, $Q_{el}$, for pyrene for all of the symmetry components as well as the total $Q_{el}$ using SE, SEP, and CC approximations. Similar to anthracene, we find that the resonance positions are shifted to lower energies in the SEP model compared to those in the SE and CC models. The magnitude of the cross section for the CC calculation is the lowest, whereas for the SE result is the highest. The reason for such behavior is already explained for anthracene (the discussion of Figure 3). Since the CC


https://dx.doi.org/10.1021/acs.jpca.0c05589
J. Phys. Chem. A 2020, 124, 7088−7100

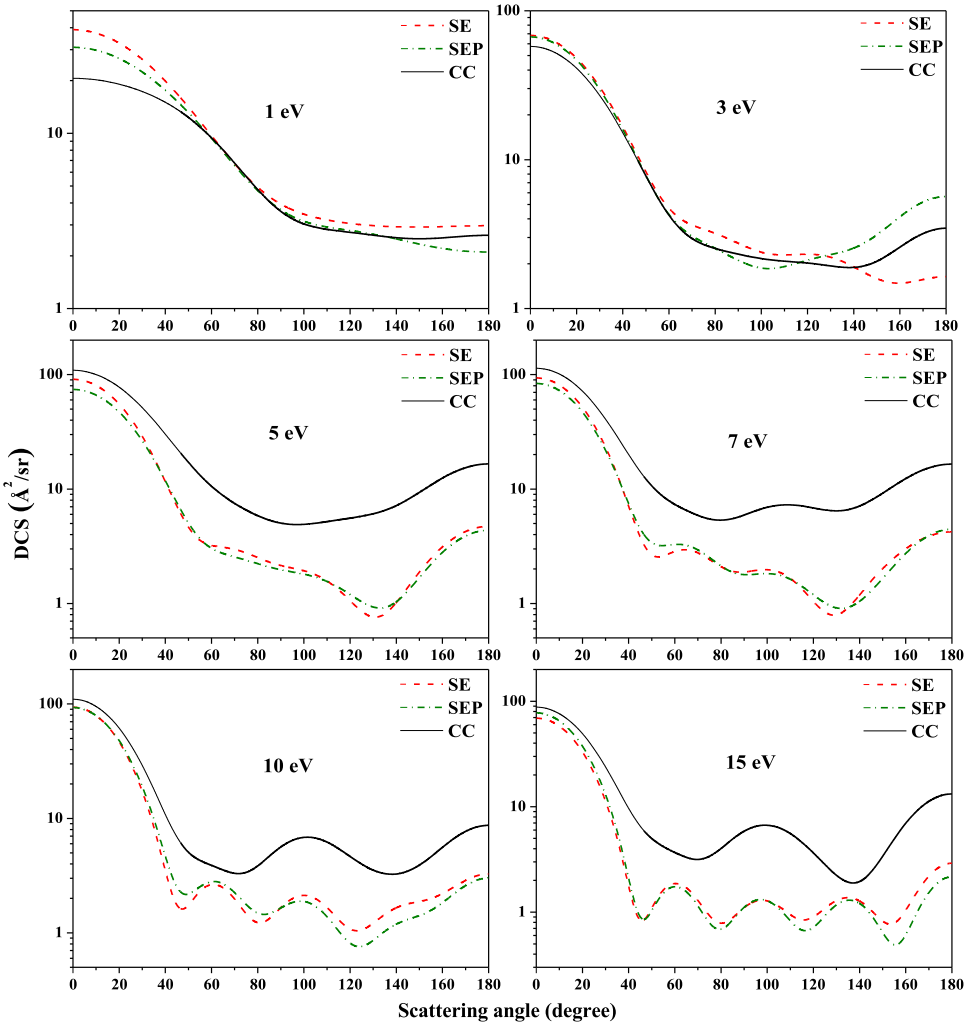


**Figure 7.** DCS for e-pyrene scattering for energies 1, 3, 5, 7, 10, and 15 eV. Dashed line, present SE approximation; dashed dot line, present SEP approximation; solid line, present CC approximation.

approximation includes excited states in the calculation, unlike the SE and SEP models, it models Feshbach/core-excited resonances quite well. The first three resonances being of shape resonance type are found in all of the three models, i.e., SE, SEP, and CC. In the CC model, these resonances are detected at 1.410, 2.237, and 2.751 eV, having respective widths of 0.022, 0.075, and 0.425 eV. In the SEP model, these resonances are observed at 1.054, 1.903, and 2.449 eV, having a width of 0.009, 0.058, and 0.283 eV, respectively, whereas in the SE model, they are seen at 1.797, 2.665, and 3.292 eV with widths of 0.028, 0.080, and 0.576 eV, respectively. In each of the models, these $\pi^*$ shape resonances are due to $^2A_u$, $^2B_{3u}$, and $^2B_{2g}$ scattering states, respectively. There are additional resonances that are detected in CC and SEP calculations and not observed in the SE calculation. In the CC calculation, these resonances are at 3.578, 5.097, and 8.36 eV for $^2B_{1g}$, $^2B_{2g}$, and $^2B_{2u}$ scattering states, respectively, whereas in the SEP calculation, these resonances are detected at energies 3.035, 4.501, and 5.368 eV for scattering states $^2B_{1g}$, $^2B_{2g}$, and $^2B_{1g}$, respectively. These resonances may be of core-excited-type shape resonances because the broader nature of these resonances makes them less likely to be of straight Feshbach type. These resonances are also visible in the $Q_{exc}$ of pyrene, which is discussed below. However, the $^2B_{1g}$ resonance occurring at 5.368 eV in the SEP calculation is not seen in the CC or SE models; hence, this could be a pseudoresonance. Apart from these two resonances, there are two resonances that are detected in both the SEP and CC calculations but not in the SE calculation. These two resonances should be Feshbach/core-excited type or mixed core-excited-type shape resonances. Furthermore, since pyrene is a polycondensed aromatic ring, it may also undergo dissociative electron attachment, as discussed for anthracene. The $\pi^*$-type shape resonance brings about a possible path of fragmentation, where a hydrogen atom is separated from the molecule (here pyrene) to form a dehydrogenated anionic radical of pyrene ($C_{16}H_9^-$). Studies such as these are very important to identify the formation of pyrene anions in the interstellar medium.

DCSs for electron scattering from pyrene at incident energies of 1, 3, 5, 7, 10, and 15 eV are shown in Figure 7 for SE, SEP, and CC models. The calculation of DCS is a stringent test for any theoretical study as it is very much sensitive to the effects that are averaged out in the integral elastic cross section. In general, DCS for pyrene with SE and SEP models overlap with each other; the reason for which is already explained earlier for anthracene. Moreover, similar to anthracene, it is seen that CC cross sections are higher than SE and SEP models. The reasonable agreement of DCS for


https://dx.doi.org/10.1021/acs.jpca.0c05589
J. Phys. Chem. A 2020, 124, 7088−7100

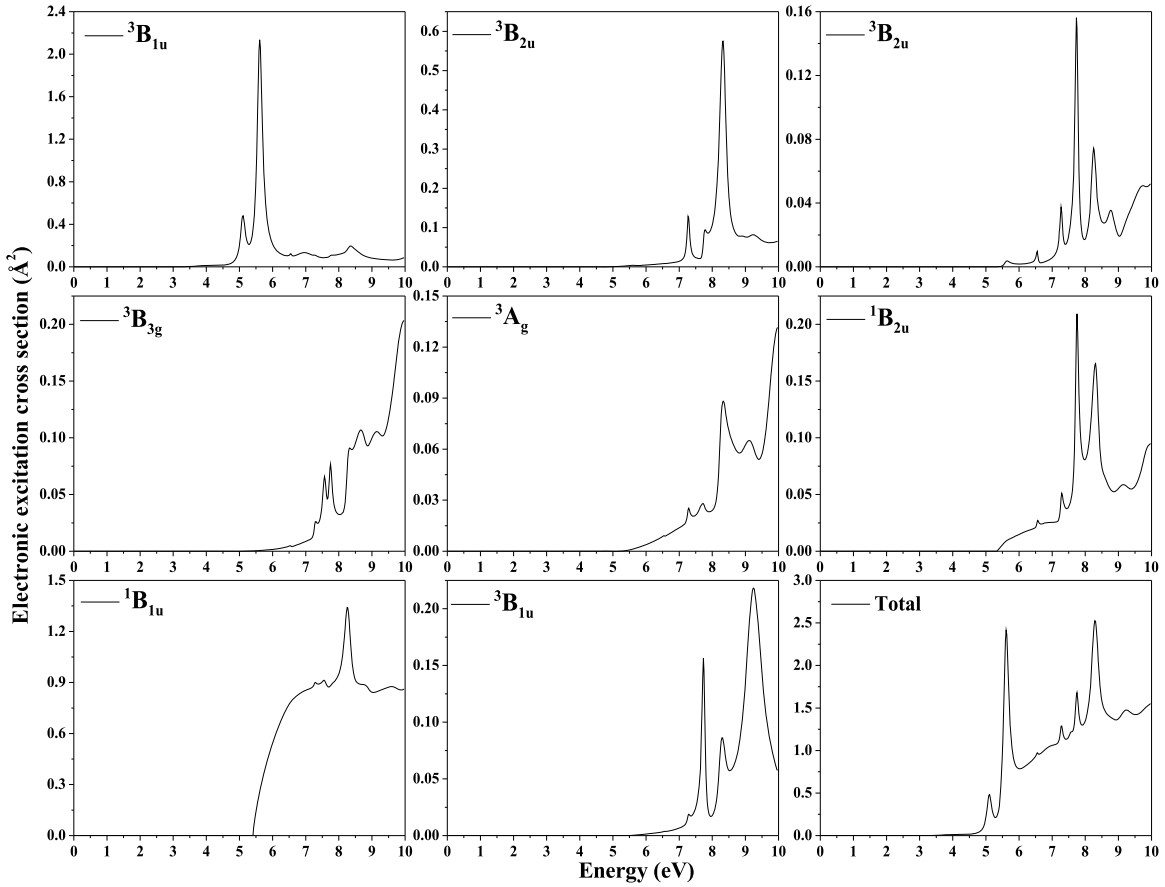


**Figure 8.** Electronic excitation cross section for pyrene for low-lying excited states. The bottom right-hand panel shows the total electronic excitation cross section.

anthracene with Sanz et al.[18] suggests that the DCS for pyrene should be reliable. The present result could be a useful guideline for future studies either experimental or theoretical. As the energy increases, close coupling of higher angular momenta of heavier inner atoms in the scattering process is observed, which sometimes results in destructive interference among various partial wave amplitudes, which is why the oscillatory nature of the curve is observed.

Figure 8 shows the electron scattering $Q_{exc}$ for the first eight excited states of pyrene. The bottom right panel shows the sum total $Q_{exc}$. Table 2 presents the vertical excitation thresholds for the first 20 states obtained in our calculations. The threshold for the first vertical excitation for pyrene is calculated to be 3.382 eV for the $^3B_{1u}$ scattering state. This scattering state has prominent peaks at 5.097 and 5.606 eV with magnitudes of 0.485 and 2.141 Å$^2$, respectively. The peak at 5.097 eV exactly matches with a $^2B_{2g}$ resonance detected in the CC calculation. Similar behavior is seen in $^3B_{2u}$ and $^1B_{1u}$ excitation cross sections. Both these cross sections have a peak at around 8.360 eV, which coincides with the position of a $^1B_{1u}$ resonance in the CC model. The set of resonances obtained in the present study above the first excitation threshold, which is seen as a sharp peak in the excitation cross sections, is expected to be of Feshbach/core-excited nature. Most of the electronically excited states have much smaller cross sections as compared to the $^3B_{1u}$ and $^1B_{1u}$ excited states, which dominate the total $Q_{exc}$.

Figure 9 shows the $Q_{ion}$ for anthracene and pyrene obtained using the BEB model[24] from the energy range of 8−5000 eV.

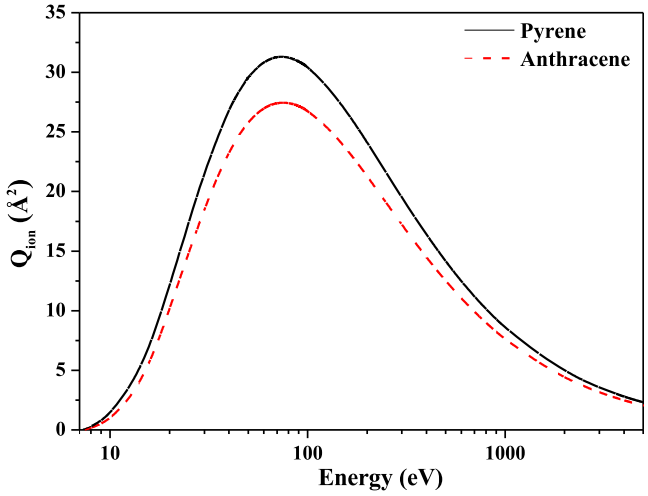


**Figure 9.** Electron impaction ionization cross section, $Q_{ion}$, computed using the BEB method.

The cross section for pyrene is higher than that for anthracene presumably due to its larger size. There are no available electron impact ionization cross sections in the literature to the best of our knowledge.

Figure 10a−10c provides a comparison between the total $Q_{el}$ for anthracene and pyrene calculated using SE, SEP, and CC approximations, respectively. The overall cross section for pyrene is greater than that for anthracene, which is expected due to its larger size. As mentioned in the Introduction section,


https://dx.doi.org/10.1021/acs.jpca.0c05589
J. Phys. Chem. A 2020, 124, 7088−7100

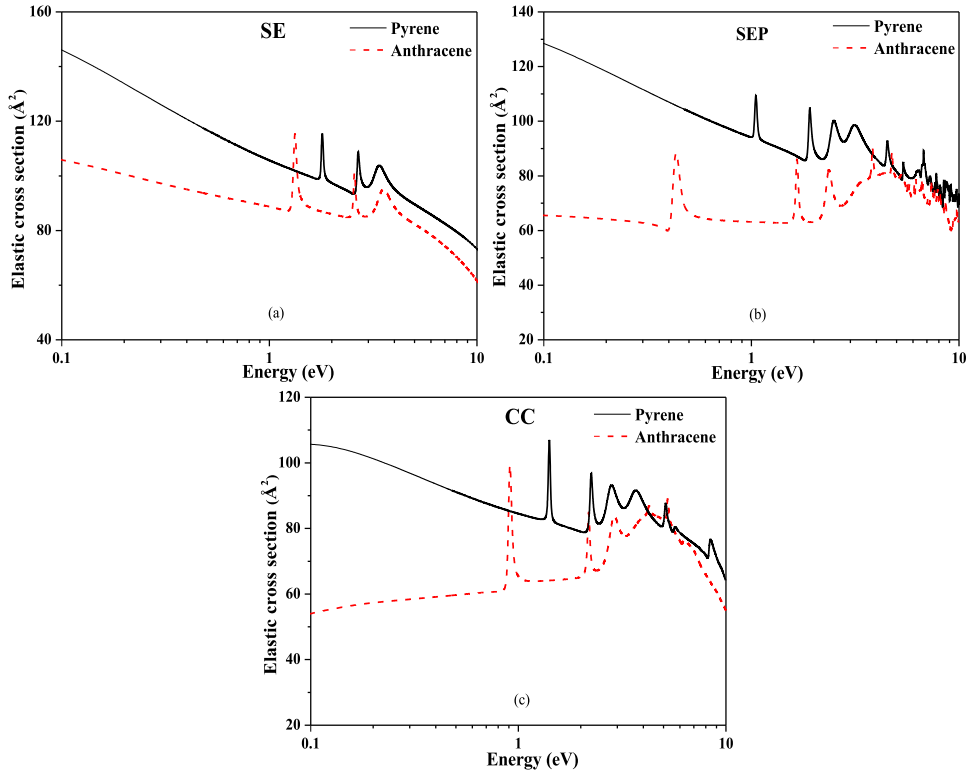


**Figure 10.** Comparison between electron scattering cross sections for anthracene and pyrene. (a) $Q_{el}$ using the SE approach, (b) $Q_{el}$ using the SEP approach, (c) $Q_{el}$ using the CC approach.

the presence of a $\pi$ bond makes the PAHs resistant to disruptions. Pyrene has more $\pi$ bonds than anthracene, which could be the reason that the resonances in pyrene are shifted to higher energies compared to those in anthracene. All of the shape resonances detected in the SE model for both the molecules are also present in SEP and CC models. In addition to that, a number of resonances are seen in SEP and CC models for both targets. Many pseudoresonances are also observed beyond 6 eV, especially in the SEP calculation. Due to the inclusion of excited states in the CC approximation, the pseudoresonances have disappeared beyond 6 eV compared to the SEP model. The nature of the cross section in all of the models is quite similar for both anthracene and pyrene.

By knowing the resonance parameters, it is possible to estimate DEA cross sections using the DEA estimator of Munro et al.[30] The estimator assumes that the molecule splits into a neutral fragment and a negatively charged fragment with known electron affinity (EA) and requires information about the bond dissociation energy (BDE) and the vibrational frequency of the dissociating mode.

We have considered that two fragmentation channels are possible: (1) $C_nH_{10} + e \rightarrow C_nH_9 + H^-$ or (2) $C_nH_{10} + e \rightarrow C_nH_9^- + H$, where $n = 14$ or 16. The threshold for DEA will be lower for the channel giving an ion with higher electron affinity; therefore, we compared the EA of the hydrogen atom (0.75 eV[31]) with the EA of the $C_nH_{10}$ fragment. For large hydrocarbon molecules, electron affinities are known to be either relatively small or indeed negative, meaning that there is no electron attachment.[32,33] We used Molpro[34] to estimate the value. HF SCF calculations give the value 0.28 eV for negatively charged anthracenide, suggesting that the dominant channel is (1), leading to $H^-$ production.

The C−H bond dissociation energy quoted by Barckholtz et al.[35] is 111 kcal/mol or 4.8 eV. The vibrational frequency for the C−H stretch used in the calculation is 3000 $cm^{-1}$.[36] The DEA cross section will have threshold energy if BDE > EA. For the PAH molecules, the threshold is 4.8−0.75 = 4.05 eV. Due to the dense resonance structure, which as shown above depends on the model employed, the threshold energy may be above or below key resonances that lie very near to this threshold. This means the results are very sensitive to the model used to determine the resonances. Figure 11 compares the results obtained using both SEP (dashed curves) and CI (solid curves) calculations.

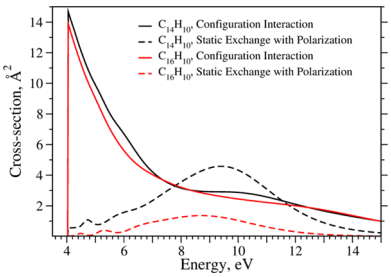


**Figure 11.** Dissociative electron attachment cross sections for anthracene and pyrene.

For both molecules, the CI method follows each other quite closely, and we suggest that their behavior is because of the wide resonances found at 3.662 eV in anthracene and at 3.578 eV for pyrene (Tables 3 and 4). The corresponding resonances found with SEP give values that lie about 0.5 eV lower; therefore, their effect on the cross sections is less significant. At higher energies, SEP calculations lead to a well-defined


https://dx.doi.org/10.1021/acs.jpca.0c05589
J. Phys. Chem. A 2020, 124, 7088−7100

Table 4. Resonance Position and Width (in eV) for Pyrene at the SE, SEP, and CC Levels of Approximation

| | present (in eV) | | | | | |
|---|---|---|---|---|---|---|
| | SE | | SEP | | CC | |
| state | energy | width | energy | width | energy | width |
| $^2A_u$ | 1.797 | 0.028 | 1.054 | 0.009 | 1.410 | 0.022 |
| $^2B_{3u}$ | 2.665 | 0.080 | 1.903 | 0.058 | 2.237 | 0.075 |
| $^2B_{2g}$ | 3.292 | 0.576 | 2.449 | 0.283 | 2.751 | 0.425 |
| $^2B_{1g}$ | | | 3.035 | 0.626 | 3.578 | 0.776 |
| $^2B_{2g}$ | | | 4.501 | 0.138 | 5.097 | 0.183 |
| $^2B_{1g}$ | | | 5.368 | 0.063 | | |
| $^2B_{2u}$ | | | | | 8.360 | 0.528 |

structure and the positions of higher-lying resonances can be seen. The two methods clearly give very different values for the DEA cross sections for these two PAHs, and a final solution to this problem will probably have to wait for a more sophisticated calculation. However, the SEP method is known to be more reliable for converging polarization effects and hence estimating the parameters of low-lying shape resonances. It would, therefore, appear likely that the SEP DEA cross sections are closer to the actual values.

## CONCLUSIONS

The UK molecular R-matrix method with SE, SEP, and CC models is implemented in this work for the calculation of various elastic and inelastic cross sections for electron scattering from anthracene and pyrene. A concise study of the DEA cross section is also performed. These astrophysically important molecules belong to the family of PAHs. Electron scattering studies on such molecular targets give many physical insights into their interaction in the ISM. Many $\pi^*$, Feshbach/core-excited, and mixed core-excited-type shape resonances are detected for both the molecules. For anthracene, the resonances detected in the present study show better agreement with the experimental results[17] than the only previous theoretical calculations by Sanz et al.[19] Many resonances are also detected for pyrene. These resonances have direct application to the process of dissociative electron attachment (DEA) studies, which is one of the key processes for understanding the selective bond breakages and dissociation mechanism of the target. As mentioned, performing experiments is quite challenging for the present set of molecules. Hence, theoretical studies such as these are very important. Since there are not many works, especially for pyrene, new studies (both theoretical and experimental) are encouraged to corroborate the present data.

## AUTHOR INFORMATION


### Corresponding Author

**Suvam Singh** − *Atomic and Molecular Physics Lab, Department of Physics, Indian Institute of Technology (Indian School of Mines), Dhanbad, JH 826004, India;* orcid.org/0000-0002-2378-1554; Email: suvamsingh18sep@gmail.com

### Authors

**Dhanoj Gupta** − *Plasma Technology Research Center, National Fusion Research Institute, Gunsan, Jeollabuk-do 54004, South Korea; Department of Particle Physics and Astrophysics, Weizmann Institute of Science, Rehovot 7610010, Israel*

**Bobby Antony** − *Atomic and Molecular Physics Lab, Department of Physics, Indian Institute of Technology (Indian School of Mines), Dhanbad, JH 826004, India;* orcid.org/0000-0003-2073-9681

**Maria Tudorovskaya** − *Department of Physics and Astronomy, University College London, London WC1E 6BT, U.K.*

**Jonathan Tennyson** − *Department of Physics and Astronomy, University College London, London WC1E 6BT, U.K.;* orcid.org/0000-0002-4994-5238

Complete contact information is available at: https://pubs.acs.org/10.1021/acs.jpca.0c05589


### Notes

The authors declare no competing financial interest.

## ACKNOWLEDGMENTS

D.G. acknowledges the support of this research from the National Fusion Research Institute (NFRI), Korea for the research grant and scholarship.

## REFERENCES


(1) Barbosa, A. S.; Freitas, T. C.; Bettega, M. H. F. Low-energy electron collisions with proline and pyrrolidine: A comparative study. *J. Chem. Phys.* **2018**, *148*, No. 074304.

(2) Jones, D. B.; da Costa, R. F.; Kossoski, F.; Varella, M. T. dN.; Bettega, M. H. F.; Ferreira da Silva, F.; Limão-Vieira, P.; García, G.; Lima, M. A. P.; White, R. D.; et al. Electron-impact electronic-state excitation of para-benzoquinone. *J. Chem. Phys.* **2018**, *148*, No. 124312.

(3) Jones, D. B.; da Costa, R. F.; Kossoski, F.; Varella, M. T. dN.; Bettega, M. H. F.; García, G.; Blanco, F.; White, R. D.; Lima, M. A. P.; Brunger, M. J. Integral elastic, vibrational-excitation, electronic-state excitation, ionization, and total cross sections for electron scattering from para-benzoquinone. *J. Chem. Phys.* **2018**, *148*, No. 204305.

(4) Loupas, A.; Lozano, A. I.; Blanco, F.; Gorfinkiel, J. D.; García, G. Cross sections for electron scattering from thiophene for a broad energy range. *J. Chem. Phys.* **2018**, *149*, No. 034304.

(5) Singh, S.; Naghma, R.; Kaur, J.; Antony, B. Calculation of total and ionization cross sections for electron scattering by primary benzene compounds. *J. Chem. Phys.* **2016**, *145*, No. 034309.

(6) Sieradzka, A.; Blanco, F.; Fuss, M.; Masin, Z.; Gorfinkiel, J.; García, G. Electron scattering from pyridine. *J. Phys. Chem. A* **2014**, *118*, 6657−6663.

(7) Vijh, U. P.; Witt, A. N.; Gordon, K. D. Small Polycyclic Aromatic Hydrocarbons in the Red Rectangle. *Astrophys. J.* **2005**, *619*, 368.

(8) Iglesias-Groth, S.; Manchado, A.; Rebolo, R.; González Hernández, J. I.; García-Hernández, D. A.; Lambert, D. L. A search for interstellar anthracene towards the Perseus anomalous microwave emission region. *Mon. Not. R. Astron. Soc.* **2010**, *407*, 2157−2165.

(9) Omont, A.; Bettinger, H. F.; Toenshoff, C. Polyacenes and diffuse interstellar bands. *Astron. Astrophys.* **2019**, *625*, A41.

(10) Lal, A. K. Origin of Life. *Astrophys. Space Sci.* **2008**, *317*, 267−278.

(11) Oettl, S.; Huber, S. E.; Kimeswenger, S.; Probst, M. Coronene and pyrene (5, 7)-member ring defects-Infrared spectra, energetics, and alternative formation pathways. *Astron. Astrophys.* **2014**, *568*, A95.

(12) Biswas, S.; Champion, C.; Weck, P. F.; Tribedi, L. C. Differential electron emission from polycyclic aromatic hydrocarbon molecules under fast ion impact. *Sci. Rep.* **2017**, *7*, No. 5560.

(13) Henning, T.; Salama, F. Carbon in the Universe. *Science* **1998**, *282*, 2204−2210.

(14) Bakes, E. L. O.; Tielens, A. G. G. M. The photoelectric heating mechanism for very small graphitic grains and polycyclic aromatic hydrocarbons. *Astrophys. J.* **1994**, *427*, 822−838.

(15) Burke, P. G.; Berrington, K. A. *Atomic and Molecular Processes−An R-matrix Approach*; Institute of Physics Publishing: Bristol, 1993.

(16) Tennyson, J. Electron−molecule collision calculations using the R-matrix method. *Phys. Rep.* **2010**, *491*, 29−76.
(17) Burrow, P. D.; Michejda, J. A.; Jordan, K. D. Electron transmission study of the temporary negative ion states of selected benzenoid and conjugated aromatic hydrocarbons. *J. Chem. Phys.* **1987**, *86*, 9−24.
(18) Sanz, A. G.; Fuss, M. C.; Blanco, F.; Carelli, F.; Sebastianelli, F.; Gianturco, F. A.; García, G. Electron scattering cross sections from anthracene over a broad energy range (0.00001−10,000eV). *Appl. Radiat. Isot.* **2014**, *83*, 68−76.
(19) Sanz, A. G.; Carelli, F.; Sebastianelli, F.; Gianturco, F. A.; Garcia, G. Dynamics of formation of anthracene anions in molecular clouds and protoplanetary atmospheres. *New J. Phys.* **2013**, *15*, No. 013018.
(20) Tennyson, J.; Brown, D. B.; Munro, J. J.; Rozum, I.; Varambhia, H. N.; Vinci, N. Quantemol-N: an expert system for performing electron molecule collision calculations using the R-matrix method. *J. Phys.: Conf. Ser. J. Phys.* **2007**, *86*, No. 012001.
(21) Gailitis, M. New forms of asymptotic expansions for wavefunctions of charged-particle scattering. *J. Phys. B: At. Mol. Phys.* **1976**, *9*, 843.
(22) Tennyson, J.; Noble, C. J. RESON−A program for the detection and fitting of Breit-Wigner resonances. *Comput. Phys. Commun.* **1984**, *33*, 421.
(23) Sanna, N.; Gianturco, F. A. Differential cross sections for electron/positron scattering from polyatomic molecules. *Comput. Phys. Commun.* **1998**, *114*, 142−167.
(24) Kim, Y.-K.; Rudd, M. E. Binary-encounter-dipole model for electron-impact ionization. *Phys. Rev. A* **1994**, *50*, 3954−3967.
(25) Faure, A.; Gorfinkiel, J. D.; Morgan, L. A.; Tennyson, J. GTOBAS: fitting continuum functions with Gaussian-type orbitals. *Comput. Phys. Commun.* **2002**, *144*, 224−241.
(26) Fujimoto, M. M.; Tennyson, J.; Michelin, S. E. Low-energy electron collisions with the alanine molecule. *Eur. Phys. J. D* **2014**, *68*, 67.
(27) CCCBDB. *Computational Chemistry Comparison and Benchmark DataBase*; NIST.
(28) Loupas, A.; Gorfinkiel, J. D. Resonances in low-energy electron scattering from para-benzoquinone. *Phys. Chem. Chem. Phys.* **2017**, *19*, 18252−18261.
(29) Stibbe, D. T.; Tennyson, J. Parent state swapping of resonances in electron-hydrogen molecule scattering. *J. Phys. B: At., Mol. Opt. Phys.* **1997**, *30*, L301.
(30) Munro, J. J.; Harrison, S.; Fujimoto, M. M.; Tennyson, J. A dissociative electron attachment cross-section estimator. *J. Phys.: Conf. Ser.* **2012**, *388*, No. 012013.
(31) Lykke, K. R.; Murray, K. K.; Lineberger, W. C. Threshold photodetachment of $H^-$. *Phys. Rev. A* **1991**, *43*, 6104−6107.
(32) Becker, R. S.; Chen, E. Extension of Electron Affinities and Ionization Potentials of Aromatic Hydrocarbons. *J. Chem. Phys.* **1966**, *45*, 2403−2410.
(33) Rienstra-Kiracofe, J. C.; Barden, C. J.; Brown, S. T.; Schaefer, H. F. Electron Affinities of Polycyclic Aromatic Hydrocarbons. *J. Phys. Chem. A* **2001**, *105*, 524−528.
(34) Werner, H.-J.; Knowles, P. J.; Knizia, G.; Manby, F. R.; Schütz, M. Molpro: a general-purpose quantum chemistry program package. *Wiley Interdiscip. Rev.: Comput. Mol. Sci.* **2012**, *2*, 242−253.
(35) Barckholtz, C.; Barckholtz, T. A.; Hadad, C. M. C-H and N-H Bond Dissociation Energies of Small Aromatic Hydrocarbons. *J. Am. Chem. Soc.* **1999**, *121*, 491−500.
(36) de Frees, D. J.; Miller, M. D.; Talbi, D.; Pauzat, F.; Ellinger, Y. Theoretical infrared spectra of some model polycyclic aromatic hydrocarbons - Effect of ionization. *Astrophys. J.* **1993**, *408*, 530.


https://dx.doi.org/10.1021/acs.jpca.0c05589
*J. Phys. Chem. A* 2020, 124, 7088−7100